Estimation of sea ice parameters from sea ice model with assimilated ice concentration and SST

Siva Prasad[1], Igor Zakharov[2], Peter McGuire[1,2], Desmond Power[2], and Richard Martin[3]

[1]Memorial University of Newfoundland, Canada
[2]C-CORE, Canada
[3]National Research Council of Canada

Correspondence to: Igor Zakharov (igor.zakharov@c-core.ca)

Abstract. A multi-category numerical sea ice model CICE along with data assimilation was used to derive sea ice parameters in the region of Baffin Bay and Labrador Sea. The assimilation of ice concentration was performed using the data derived from Advanced Microwave Scanning Radiometer (AMSR-E & AMSR2). The model uses a mixed layer slab ocean parametrization to compute the Sea Surface Temperature (SST) and thereby to compute the potential to freezing/melting of ice. The data from Advanced Very High Resolution radiometer (AVHRR-only OISST analysis) was used to assimilate SST. The modeled ice parameters including concentration, ice thickness, freeboard, and keel depth were compared with parameters estimated form remote sensing data. The ice thickness estimated from the model was compared with the measurements derived from Soil Moisture Ocean Salinity - Microwave Imaging Radiometer using Aperture Synthesis (SMOS-MIRAS). The model freeboard estimates were compared with the freeboard measurements derived from CryoSat2. The ice concentration, thickness and freeboard estimates from model assimilated with both ice concentration and SST were found to be within the uncertainty of the observation except during March. The model estimated draft was compared with the measurements from an upward looking sonar (ULS) deployed in the Labrador Sea (near Makkovik Bank). The difference between modeled draft and ULS measurements estimated from the model was found to be within 10 cm. The keel depth measurements from the ULS instruments were compared to the estimates from the model to retrieve a relationship between the ridge height and keel depth.

1 Introduction

Regional sea ice forecast is important for climate studies, operational activities including navigation, exploration of offshore mineral resources, and ecological applications, e.g. North Water polynya in Baffin Bay provides a warm environment for marine animals (Stirling, 1980).

Sea ice is a heterogeneous media and makes it practically difficult for remote sensing instruments to measure the ice thickness, freeboard, and ridge parameters (Carsey, 1992). The climate forecast researchers and operational ice modeling communities depend on numerical modeling techniques implementing the physical process of atmosphere and ocean on large scale computational platforms along with data assimilation methods to retrieve the information on sea ice parameters. Data assimilation methods can provide more accurate initial conditions for forecasting systems (Caya et al., 2006, 2010). The estimation of sea ice parameters is a challenging problem in the region of Baffin Bay and the Labrador Sea due to the high interannual variability of sea ice in this area (Fenty and Heimbach, 2013).

Previous sea ice modeling and assimilation studies at the Canadian Ice Service (CIS) (Sayed et al., 1999) provided an overview of an operational ice model coupled with atmospheric and ocean modules. The research (Sayed et al., 2001) compared the evolution of ice thickness distributions followed by the development of an operational ice dynamics model for CIS (Sayed et al., 2002). The CIS used the model developed by (Sayed et al., 1999, 2002) was used to study the ice thickness distribution in the Gulf of St. Lawrence (Kubat et al., 2010) These modeling works were also improved by the data assimilation methods (Caya et al., 2006, 2010). The Community Ice Ocean Model (CIOM) by Caya et al. (2006) used the Princeton Ocean Model for the simulation of ocean parameters and a multi-category ice model. The total ice fraction retrieved from the Special Sensor Microwave/Imager (SSM/I) was assimilated into CDOM using 3D variational (3DVAR) technique (Caya et al., 2006) to estimate the ice concentration. The ice concentration estimates were further improved by assimilating information from both daily ice charts and RADARSAT (Caya et al., 2010). Assimilation studies by Lindsay (Lindsay and Zhang, 2006) showed significant improvement in assimilated ice concentration but with a large bias in the ice thickness pattern.

Karvonen et al. (2012) presented a method for ice concentration and thickness analysis by combining the modeling of sea ice thermodynamics and the detection of ice motion by space-borne Synthetic Aperture Radar (SAR) data from RADARSAT-1 and RADARSAT-2. The method showed promising results for sea ice concentration and ice thickness estimates. In another study, Ocean and Sea Ice Satellite Application Facility (OSI SAF) data were assimilated into Regional Ocean Modeling System (ROMS) for simulating sea ice concentration and produced better results than the simulation without assimilation (Wang et al., 2013). Ice concentration and extent were overestimated in the assimilated model, probably due to the bias in atmospheric forcing, underestimation of heat flux and over/under estimation of sea ice growth/melt processes.

Sea ice models can be coupled to ocean and atmosphere models, but they can also be run in a standalone mode by prescribing the atmospheric and ocean conditions. The literature does not provide details and discussion on regional implementation and results for stand-alone models. The 3D-CEMBS is an eco-hydrodynamic model that includes a coupled POP-CICE model for operational forecasting implementation of CICE on a regional scale. The implementation on the regional scale of the ice component and the validation work is still ongoing (Dzierzbicka-Głowacka et al., 2013). The advantage of the sea ice model, CICE version 5.1.2 (Hunke et al., 2015) is the standalone capability. Here we use a combination of modeling using the stand alone sea ice model, CICE, and the combination of optimal interpolation and nudging methods (Lindsay and Zhang, 2006; Wang et al., 2013) to assimilate ice concentration. The optimal interpolation and nudging method is also used to assimilate SST estimated by a slab ocean parametrization in the sea ice model. The optimal interpolation method is computationally inexpensive and was shown to provide better estimates than non-assimilated model (Wang et al., 2013). The simulated sea ice parameters are then validated with the observations in the region of the Baffin Bay and the Labrador Sea. This work uses a high-resolution model configuration which was previously described in the work of (Prasad et al., 2015). The changes in ice concentration were taken into account to estimate the changes in the ice volume and thereby thickness estimates. The ice prediction models such as Regional Ice Prediction System (RIPS) (Lemieux et al., 2016) limits the discussion on ice concentration estimates from the model. In this work, in addition to validation of the ice concentration we also discuss the effect of the assimilation on ice thickness, freeboard, draft and keel depth. Since freeboard, draft and keel are functions of ice concentration and ice volume it is reasonable to compare the model values with corresponded observations. The work suggests a methodology to extract the level ice draft and keel depth information from ULS measurements, which was then used to describe the relationship between ridge and keel.

2 Model domain and forcing data

The sea ice model was implemented on a regional scale of about 10 km orthogonal curvilinear grids with a slab ocean mixed layer parameterization. Density-based criteria were used as in (Prasad et al., 2015) to compute the mixed-layer depth and thereby compute the SST and the potential to grow or melt sea ice. The assessment of the non-assimilated model of the sea ice concentration and its seasonal means showed that the error associated with the model mostly spread across the area of the North Water polynya and the Davis Strait where the interaction of cold and warm water is frequent. In the present study, a data assimilation module is also introduced.

The surface atmospheric forcing is from high-resolution North American Regional Reanalysis (NARR) data (Mesinger et al., 2006). The ocean forcing is from various sources: currents from Climate Forecast System Reanalysis (CFSR), salinity from World Ocean Atlas, WOA-2013 (Levitus et al., 2013) and Mixed Layer Depth (MLD) computed from WOA-2013 (Prasad et al., 2015). (Prasad et al., 2015) used a density criteria of 0.2 Kg/m^3 at 10m depth, the other models such as RIPS by CIS (Lemieux et al., 2016) uses a density criteria of 0.01 Kg/m^3 from the ocean surface. Atmospheric and ocean forcing were used as inputs to the model. For Sea Surface Temperature (SST), a monthly climatology data derived from high-resolution NOAA were used as an input for the initial and boundary conditions. The net heat flux from the atmosphere is the upper boundary condition for ice thermodynamics. The heat flux from the ocean to the ice is the lower boundary condition. Based on temperature profile and boundary conditions the melt and growth of ice is computed. The open boundaries are configured in the same way as in (Hunke et al., 2015; Prasad et al., 2015). For the ice concentration and thickness, the initial condition is assumed as a no-ice state at the beginning of September 2004. The data assimilation starts from January 2005 and continually assimilated whenever data was available.

3 Remote Sensing Data for Assimilation and Validation

Ice concentration derived from AMSRE of resolution 6×4 km (Spreen et al., 2008) were used for the assimilation of ice concentration. AMSRE was developed by JAXA, and it is deployed on Aqua satellite. AMSRE and AMSR2 are passive sensors that look at the emitted or reflected radiation from the earth's surface with multiple frequency bands. The vertical (V) and horizontal (H) polarization channels near 89 GHz were used to compute the ice concentration from AMSRE (Spreen et al., 2008). The Arctic Radiation and Turbulence Interaction STudy (ARTIST) sea ice algorithm used to determine ice concentration from AMSRE show excellent results above 65% ice concentration where the error does not exceed 10%. With low ice concentrations, substantial deviations can occur depending on atmospheric conditions. The parameters of the sensor are provided in Table 1. AMSRE ice concentration were available from January 2005 to September 2011, after which it stopped functioning. From August 2012 AMSR2 had been used for data collection. The same frequency (89 GHz) as that of the AMSRE instrument was used to derive information from AMSR2. The spatial resolutions also remain the same for both AMSRE and AMSR2. The same algorithm was applied to derive ice concentrations from both AMSRE and AMSR2. The original AMSRE/AMSR2 data with 6×4 km resolution scale were interpolated to the model grid before assimilation.

Table 1. Specifications of microwave radiometers used to estimate ice concentration.

Specifications	AMSR-E	AMSR2	SSMIS	
Center Frequency, GHz	89	89	19	37
Mean Spatial resolution, km	6×4	5×3	69×43	37×28
Polarization	HV	HV	V	HV
Incidence angle, deg	55	55	50	
Swath, km	1445	1450	1700	
Data availability, month/year	$08/2002 - 10/2011$	08/2012-Present	$03/2005-$Present	

The assimilated model results of ice concentration were compared with the OSI SAF data. The details of the sensors are given in Table 1. The OSI SAF product is derived from Special Sensor Microwave Imager Sounder (SSMIS) (Tonboe et al., 2016; Bell, 2006). The data is available on a 10 km polar stereographic grid and are derived from 19 V, 37 VH channels. The erroneous data, were the ice concentration error was 100% or retrieval algorithm has failed were filtered out before the comparison. Measurements derived from AVHRR-only OISST analysis (Reynolds et al., 2007; Smith, 2016) were used for SST assimilation. SST data products are generated using a combination of satellite and in situ observations from buoy and ship observations and is available on a $0.25° \times 0.25°$ resolution. The analysis product estimates SST from ice concentration only in regions where ice concentration is greater than 50%, otherwise uses satellite data to retrieve SST values.

Freeboard measurements from CryoSat-2 altimeter were used to compare the freeboard estimates by the model. CryoSat-2 altimeter operating in the SAR mode, SIRAL has the accuracy of about 1 cm with the spatial sampling about 45 cm (Bouzinac, 2014). The pulse limited footprint width in the across track direction is about 1.65 km and beam limited footprint width in the along-track direction is about 305 m (Scagliola, 2013), that corresponds to an along-track resolution about 401 m (assuming flat-Earth approximation). Therefore, the pulse-Doppler-limited footprint for SAR mode is about 0.6 km^2. The CryoSat-2 freeboard and the ice-concentration products were generated at Alfred Wegener InstInstitute (AWI) (Ricker et al., 2014). The products are available in a spherical Lambert azimuthal equal-area projection of 25 km resolution cell. The uncertainty of freeboard measurements can arise from speckle noise, lack of leads which causes the estimation of sea surface height unreliable, and snow cover. The uncertainty up to 40 cm can be observed in the region of Baffin Bay and Labrador Sea (Ricker et al., 2014).

For ice thickness, data product derived from the SMOS Microwave Imaging Radiometer with Aperture Synthesis (MIRAS) instrument (1.4-GHz channel) (Kaleschke et al., 2012) on a grid resolution of $12.5x12.5$km is used. The ice thickness is retrieved from observation of the L-band microwave sensor of SMOS. Horizontal and vertical polarized brightness temperatures in the incidence range of $< 40°$ are averaged. The ice thickness is then inferred from a three layer (ocean-ice-atmosphere) dielectric slab model. SMOS data are available from 15 October 2010. The presence of snow accumulated over months also can increase the uncertainty. The uncertainty of SMOS ice thickness (observations) shown in Table 2 (Tian-Kunze et al., 2014; Ricker et al., 2016; Tietsche et al., 2017, 2018) includes the error contributions, which are caused by the brightness temperature, ice temperature and ice salinity. The insufficient knowledge of the snow cover also introduces a large uncertainty in ice thickness estimates. Snow depth uncertainity can be $50-70\%$ of mean value (Zhou et al., 2018). In general, the uncertainty of thickness observation increases with increasing ice thickness, increasing snow cover and the onset of melt (Kaleschke et al., 2013). The SMOS ice thickness retrieval produces large uncertainty during the melt season and hence retrieval is not conducted during the melt season. Table 3 shows the details on SMOS sensor (Kerr et al., 2001; Barré et al., 2008).

ice thickness (observations) shown in Table 2 include.

Table 2. SMOS uncertainty

Ice thickness	Uncertainty caused by a standard deviation of		
	0.5 K temperature brightness	1 K ice tempearture	1 g/Kg ice salinity
0 -10 cm	$<$ 1 cm	$<$ 1cm	$<$ 1cm
10-30 cm	$<$ 1 cm	1-5 cm	1- 13 cm
30-50 cm	1-4 cm	2-10 cm	2-22 cm
$>$ 50 cm	$>$ 4cm	$>$ 7cm	$\leq$ 40 cm

Table 3. SMOS sensor specifications.

Polarization	HV
Incidence angle	$0-55°$
Swath, km	900
Center Frequency (GHz)	1.4 (L-band)
Mean Spatial resolution (km)	$35-50$
Radiometric sensitivity over ocean, K	2.5 and 4.1

Ice draft measurements from an ULS instrument (Ross et al., 2014) located on the Makkovik Bank, see Figure1, at $58.0652°$ W and $55.412°$ N, were used to analyze the ridge keel and the level ice draft in the region.

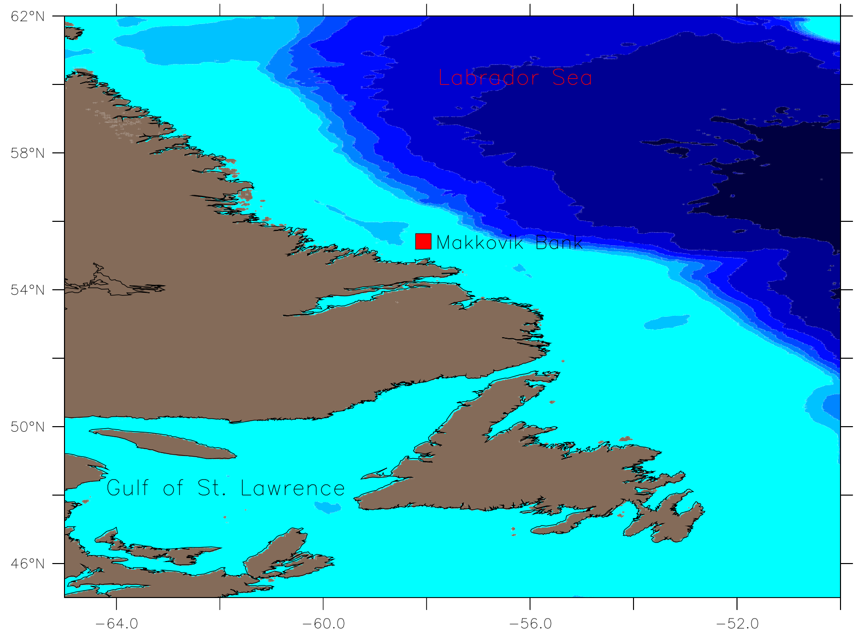

Figure 1. The location of ULS instrument.

The ULS data measured at an interval of approximately 5.5 seconds is available from the beginning of January to end of May during 2005, 2007 and 2009. The frequency histogram of the data yields a uni-modal, bi-modal or multi-modal distribution. A sample histogram is provided in Figure 2, for 10 February 2007. We assume that the first mode in the histogram corresponds to the level draft ice and the second mode corresponds to the ridge keel measurement. The first mode of the distribution is selected by finding a minimum between two peaks. The histogram was analyzed to derive daily averages of ice draft and keel measurements (Prasad et al., 2016).

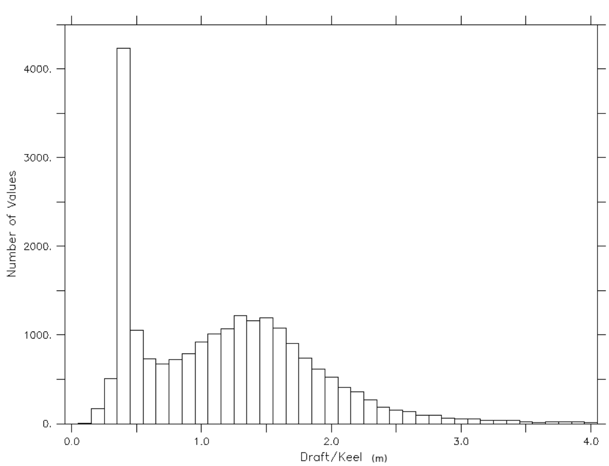

Figure 2. The histogram of the ULS measurement, 10 February 2007 for the estimation of draft and keel (meters).

4 Data Assimilation

The assimilation module uses a combined optimal interpolation and nudging technique for ice concentration (Lindsay and Zhang, 2006; Wang et al., 2013). The method can be represented generally as equation (1) (Deutch, 1965; Lindsay and Zhang, 2006).

$$X_a = X_b + dt\frac{K}{\tau}(X_o - X_b), \tag{1}$$

where X_a is the final analysis of the variable, X_o is the observed quantity (for ice concentration this is AMSR-E/AMSR2, for SST this is AVHRR-only OISST), X_b is the background estimate of the variable (for ice concentration and SST this is model estimate), dt is the model time step, τ is the basic nudging time scale as in (Wang et al., 2013), and K is the nudging weight with the optimal interpolation value. K is computed as

$$K = \frac{\sigma_b^\alpha}{\sigma_b^\alpha + \sigma_o^2}, \tag{2}$$

where σ_b and and σ_o are the error standard deviation of the model estimate (Deutch, 1965) and the observations (Deutch, 1965) respectively The parameters in the weighing factor given in equation (2) is defined according to (Lindsay and Zhang, 2006) as $\sigma_b = |X_o - X_b|$; $\sigma_o = 0.08$ (parameter may vary spatially), $\alpha = 6$.

When assimilation of ice concentration, $\sigma_o = 0.08$ is calculated from a long-term standard deviation to 0.08 since the AMSR-E/AMSR2 ice concentration error is depends on various atmospheric conditions for values less than 65%. The parameter $\alpha = 6$, is used for the present study to ensure that the coefficients for assimilation are heavily weighted only when there is large variation between the model and the observation (Lindsay and Zhang, 2006).

SST is also assimilated using the nudging and optimal interpolation scheme. For SST assimilation, σ_o is fixed as 0.05 to compensate for the assumption of zero mixed layer heat flux. A value α equal to 6 (Lindsay and Zhang, 2006) was also used for the assimilation of SST to ensure that only large differences between the model and observation are weighted heavily

The assimilation of ice concentration is then followed by a re-computation of the estimated sea ice volume. The ice volume is subtracted or added by including the increments or decrements with specified ice thickness. Since a variable drag coefficient has been used for the friction associated with an effective sea ice surface roughness at the ice-atmosphere and ice-ocean interfaces and to compute the ice to ocean heat transfer the level ice area is updated by assuming the model deformed ice area and volume represents the realistic values.

5 Results and validation

Three model results are discussed here: model ‘M0’, the non-assimilated model; ‘M1’, the model assimilated with ice concentration from AMSR-E/AMSR2; and ‘M2’, the model assimilated with ice concentration from AMSR-E/AMSR2 and SST from AVHRR-only OISST. ‘M2’assimilates only SST whenever there is a data gap in ice concentration from AMSR-E (e.g. from 24

March 2005 to 31 March 2005), AMSR-E data are not available and, in that case, 'M2'assimilates SST instead of ice in data gaps. The AMSR-E instrument stopped producing data since October 2011, and AMSRE2 data has been used for assimilation beginning August 2012. The model was spin up for 3 months before assimilation, since no coupling with ocean model is done, the spinup time of 3 months is enough to estimate the ice conditions.

5.1 Ice concentration

Figure 3 column 1 shows the absolute mean difference of ice concentration between the non-assimilated model and the OSI SAF data, column 2 shows the absolute mean difference of ice concentration of the model assimilated only with ice concentration and OSI SAF data, and column 3 shows absolute mean difference of ice concentration of the model assimilated with both ice concentration and SST and OSI SAF data. Model M2 shows improvement in the ice concentration for January and March, but little improvement between M1 and M2 for May 2010.

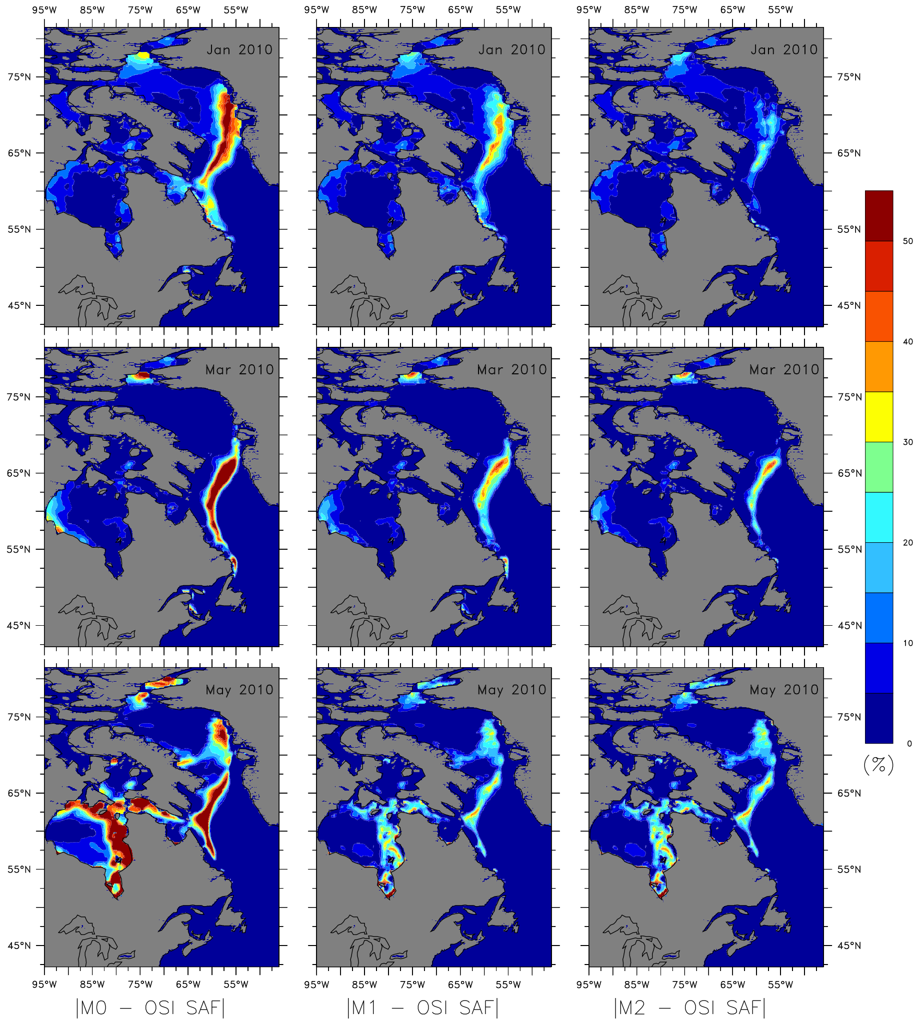

Figure 3. The absolute mean difference of ice concentration of ice concentration from non-assimilated, assimilated models and OSI SAF data for Jaunary 2010, March 2010 and May 2010.

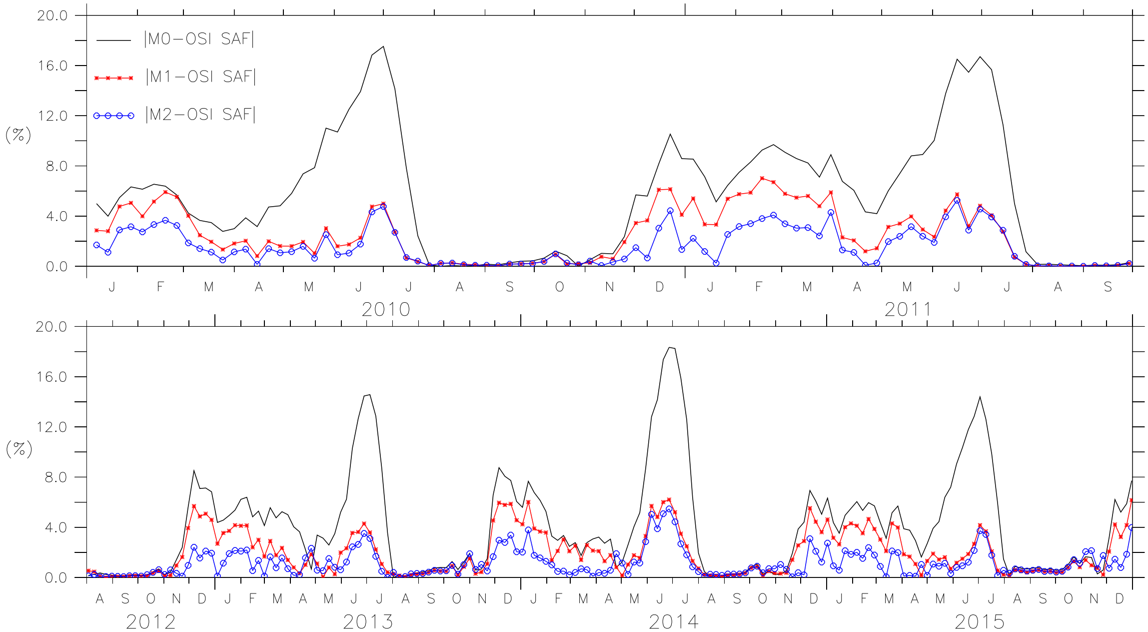

Figure 4. The absolute mean difference of ice concentration for models M0, M1 and M2 from January 2010 to September 2011 is shown in row 1 and from August 2012 to December 2015 is shown in row 2.

Figure 4 shows the absolute mean difference of ice concentration of the model assimilated with AMSR-E/AMSR2 and OSI SAF (SSMIS) data from January 2010 to September 2011 and the absolute mean difference of ice concentration from August 2012 to December 2015. The assimilation of SST and ice concentration decreases the error between the model and the OSI SAF ice concentration. In 2010, the non-assimilated model error of 4.624% was reduced to 1.939% by assimilating ice concentration. The assimilation of SST and ice concentration decreased the error to about 1.118% in 2010.

From October 2011 to July 2012, AMSR-E data are not available for a more extended period, and model M2 was assimilated only with SST, see Figure 5. During this period, the SST assimilation decreases the error between the model and the observation by almost 3%.

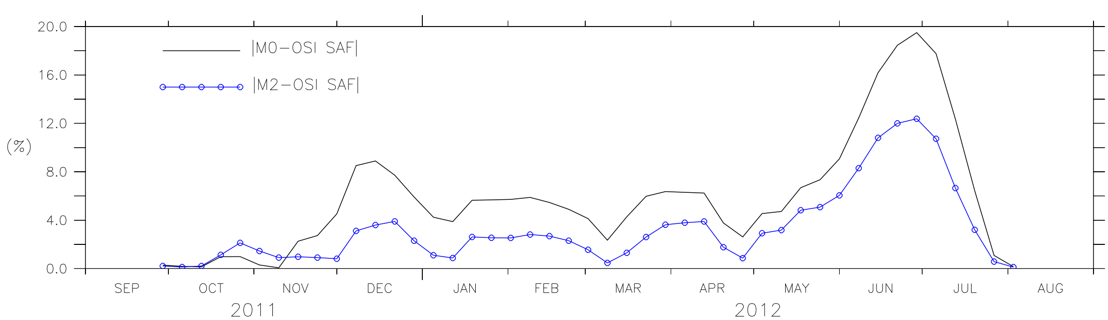

Figure 5. The absolute mean difference of ice concentration from October 2011 to July 2012, ice concentration was not available for assimilation and hence model M2 will be only assimilated with SST during the period.

5.2 Ice thickness

In this section, we perform the comparison of ice thickness from the model with the observation. The large unacceptable uncertainties in observation data derived from SMOS create difficulties for the analysis. Also, it is strictly recommended not to use the SMOS data with an uncertainty greater than one meter (Tian-Kunze and Kaleschke, 2016) for practical applications. For comparison and validation, ice thickness data from both the model and observation where the observed ice thickness has an uncertainty less than or equal to 100 cm are selected.The SMOS thickness has less uncertainty for thinner ice and higher uncertainty for thicker ice, see Table 2 for the uncertainty of SMOS ice thickness. In the case of SMOS derived thickness, the uncertainties would increase with the snow accumulation and melt onset.

Figures 6, 7, 8 shows the mean values of the thickness estimated from models M0, M1, M2 and SMOS with the uncertainty limits of the SMOS ice thickness (shaded gray)As ice thickness increases through the season, so do the uncertainty limits. The values of Model M2 are within the uncertainty limits of SMOS ice thickness from October until the end of February (except for 2014) end. From the comparison, during March, the model results exceed the uncertainty limits. Figure 8 shows the results for the period October 2011 to April 2012 where AMSR-E data were missing during which M1 was not assimilated with ice concentration but used the initial conditions from the assimilated result. Model M2 used the initial conditions assimilated with both ice concentration and SST but assimilates only SST during the period. Both models, M1 and M2, with the improved initial conditions show better forecasts in the long-term analysis. One of the reasons why the model values exceed the uncertainty limits during March is the choice of $\alpha = 6$, which considers only large differences while weighing the coefficient K. Since the assimilation shows improvement in ice thickness, using a value of $\alpha = 2$, it is expected to impose the model values within the uncertainty limits.

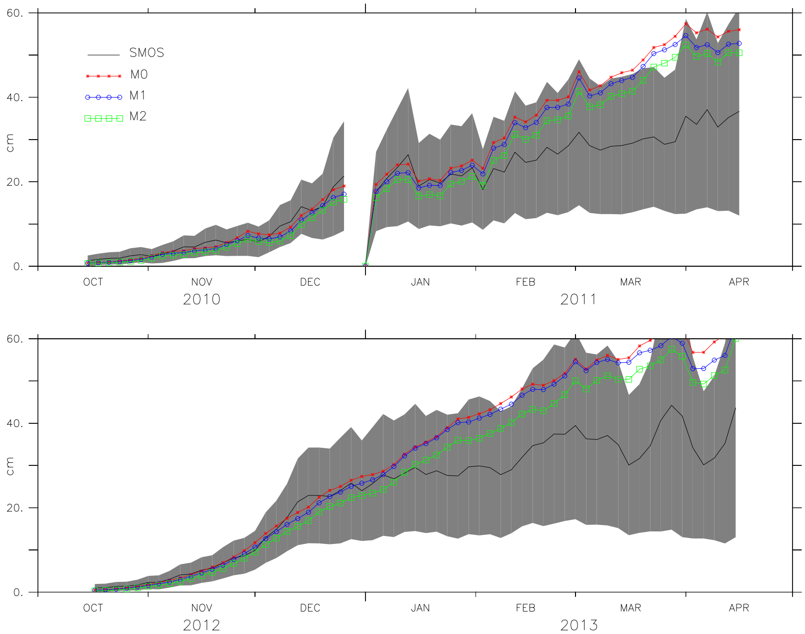

Figure 6. The ice thickness from the models M0, M1, M2, and observation (SMOS ice thickness) from October 2010 to April 2011 and October 2012 to April 2013 . The uncertainty of observation (SMOS ice thickness) is shaded in gray.

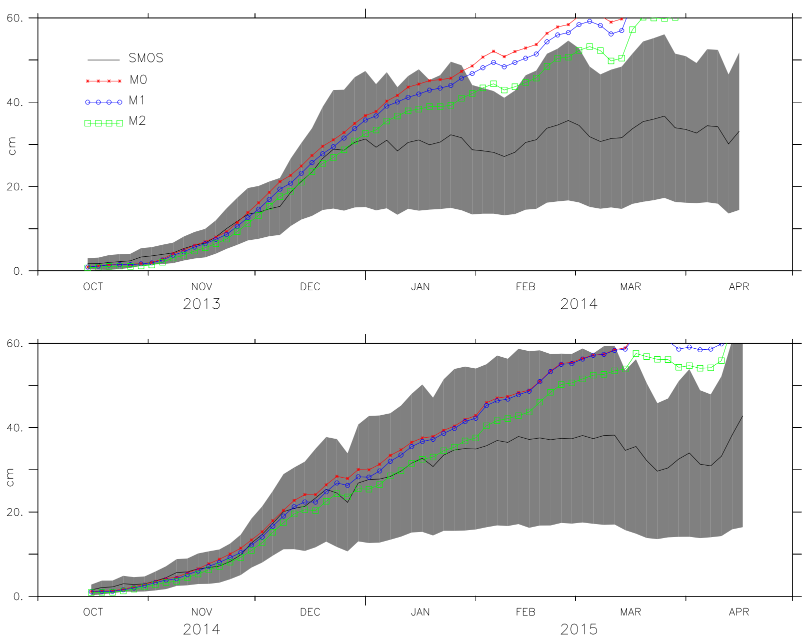

Figure 7. The ice thickness from the models M0, M1, M2, and observation (SMOS ice thickness) from October 2013 to April 2014 and October 2014 to April 2015. The uncertainty of observation (SMOS ice thickness) is shaded in gray.

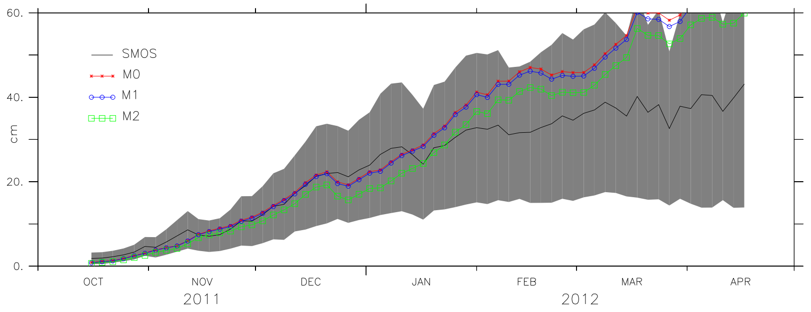

Figure 8. The ice thickness from models M0, M1(not assimilating ice concentration as there were no AMSRE data available, but used the initial conditions from the model assimilated with ice concentration), M2 (assimilated only with SST and used model initial conditions derived from assimilating both ice concentration and SST) and observations (SMOS ice thickness) from October 2011 to April 2012. The uncertainty of observation (SMOS ice thickness) is shaded in gray.

The Model M2 thickness, SMOS derived ice thickness, and the uncertainty of the SMOS derived measurement for 15 December 2010, 15 January 2011 and 15 March 2011 are shown in Figure 9, and includes regions where observed uncertainties are larger than one meter.

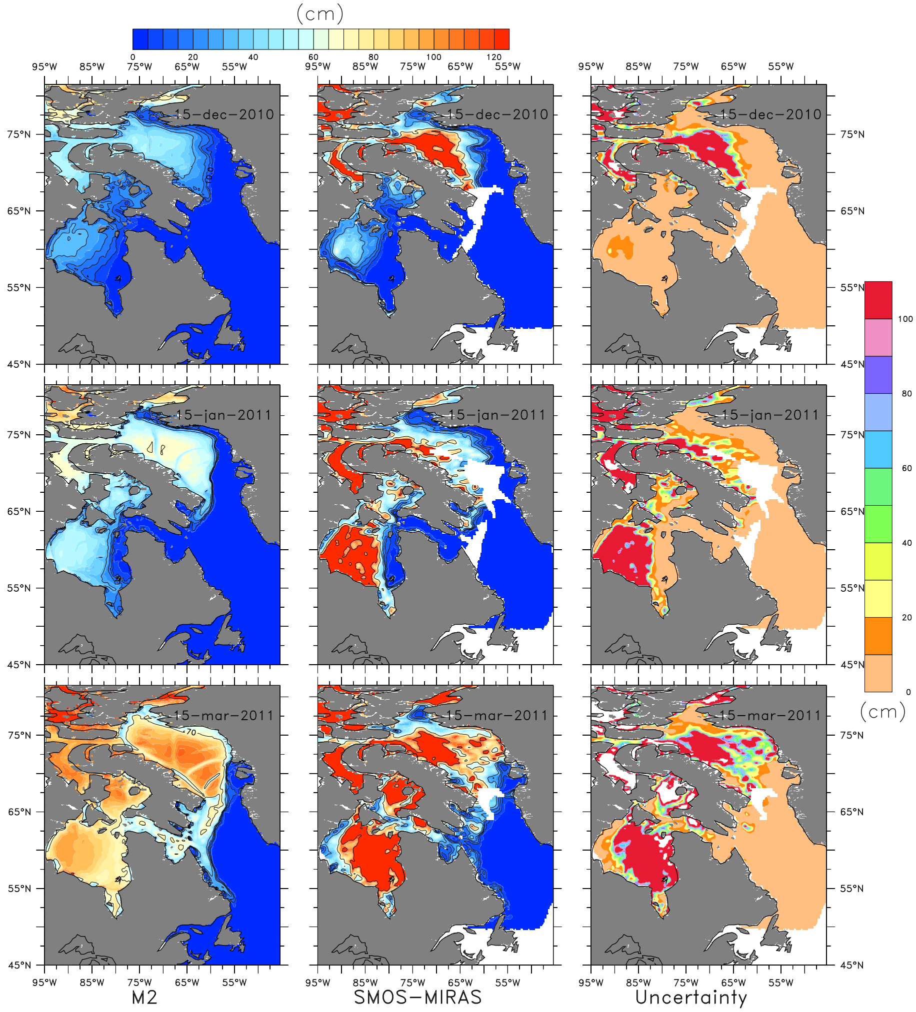

Figure 9. The model 'M2' estimated ice thickness, SMOS-MIRAS derived ice thickness, and the observation uncertainty for 15th December 2010, 15th January 2011 and 15th March 2011.

The thickness results for thin ice categories (< 30 cm)from the model with SMOS are shown in Figures 10, 11, and 12, the shaded region shows the uncertainty of the thin ice from SMOS data. The thin ice category thicknesses are overestimated from October to November end but the values are within the uncertainty limits of SMOS from December to March.

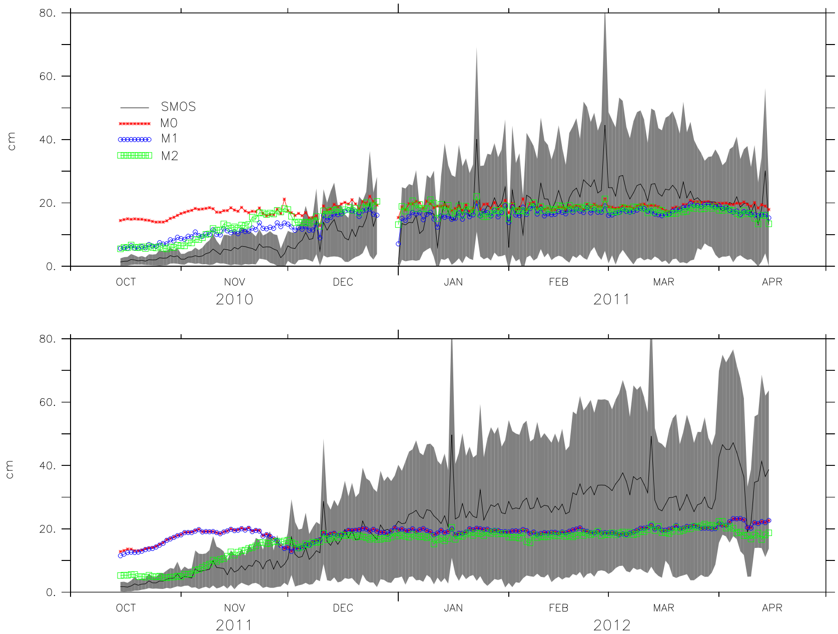

Figure 10. The ice thickness from the models M0, M1, M2, and observation (SMOS ice thickness) and the observation uncertainty (shaded gray) for SMOS ice thickness less than 30 cm (2010 - 2012).

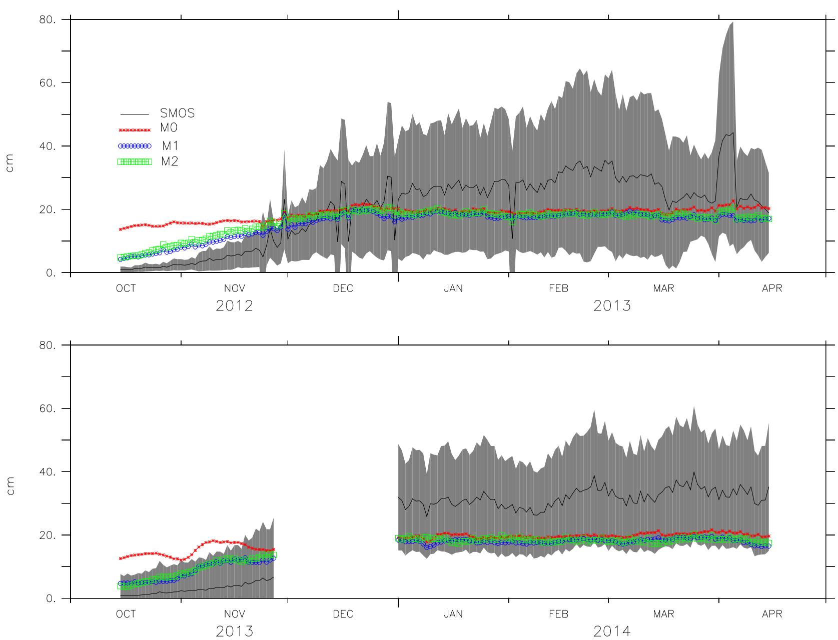

Figure 11. The ice thickness from the models M0, M1, M2, and observation (SMOS ice thickness) and the observation uncertainty (shaded gray) for SMOS ice thickness less than 30 cm (2012 - 2014).

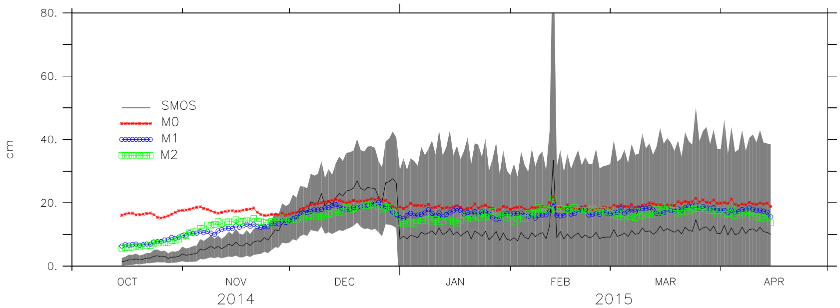

Figure 12. The ice thickness from the models M0, M1, M2, and observation (SMOS ice thickness) and the observation uncertainty (shaded gray) for SMOS ice thickness less than 30 cm (2014 - 2015).

Figure 13, shows the SST from AVHRR-only OISST analysis with the shaded regions representing the observation uncertainty, SST from models M0, M1 and M2. In general, the SST from AVHRR-only OISST assimilation improves the ice concentration and ice thickness results for the model M2. The assimilated model M2 still has systematic bias during the summer and winter, which may be improved by decreasing choice of α (=6, presently) and by decreasing the nudging time scale (presently for SST nudging scale is 30 days). Decreasing the nudging time scale can result in the late formation and early melt of ice (not shown here). The results can be improved with a choice of nudging time scale to be less frequent during the formation and more frequent during the winter till beginning or mid of March. Frequent nudging is also found to produce blow up for the thermodynamic model. Choice of the parameters in the assimilation has to be selected so that balance is maintained not to cause late formation and earlier melt and maintain the stability of the model thermodynamics and dynamics. For M0, non-assimilated model the results may be improved by including the mixed layer heat flux with a parametrization similar to (Petty et al., 2014). Also, note that the model still assumes a fixed salinity profile and mixed layer profile.

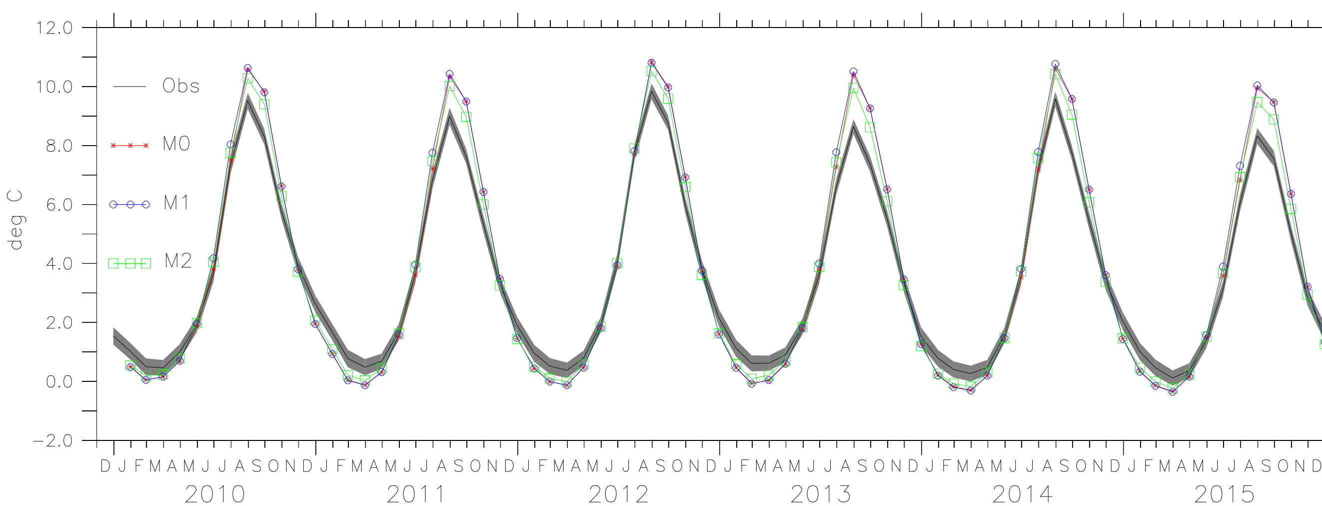

Figure 13. The SST from AVHRR-only OISST analysis with the shaded region represents the uncertainty of AVHRR-only OISST analysis, and SST from models M0, M1, M2.

5.3 Draft and keel depth

The ULS measurements were separated into level ice draft and keel depth measurement as described in Prasad et al. (2016) and also in Section 3. The level ice draft, D is computed using equation (3) (Tsamados et al., 2014). The results are shown in Figure 14.

$$D = (\rho_i v_{ice} + \rho_s v_{sno})/(A\rho_w) \tag{3}$$

Where $\rho_i = 917kg/m^3$ is the density of ice, v_{ice} is the volume of ice, $\rho_s = 330.0kg/m^3$ is the density of snow, v_{sno} is the volume of snow, A is ice concentration, $\rho_w = 1026kg/m^3$ is the density of sea water.

Some deviations are noticed in the comparison of level ice draft. The estimated absolute error is about 10 cm for 2005, 2007, 2009. The error of 10cm on draft of 20 cm can be accepted considering large difference in spatial resolution between the ULS and Model. Also, the analysis was done only for 2005, 2007, 2009 as this was when data was available.The discrepancy occurs due to the fact that ULS gives values at a particular location with high resolution (within the footprint of several meters), while the model is of 10 km resolution gives an averaged result close to the location of the ULS. Moreover, the analysis of histogram from ULS shows multi-modal distribution at certain time points which indicates the presence of rafted ice. In the present study, the rafted ice is also included and considered as the ridges which contribute towards the results achieved in this section.

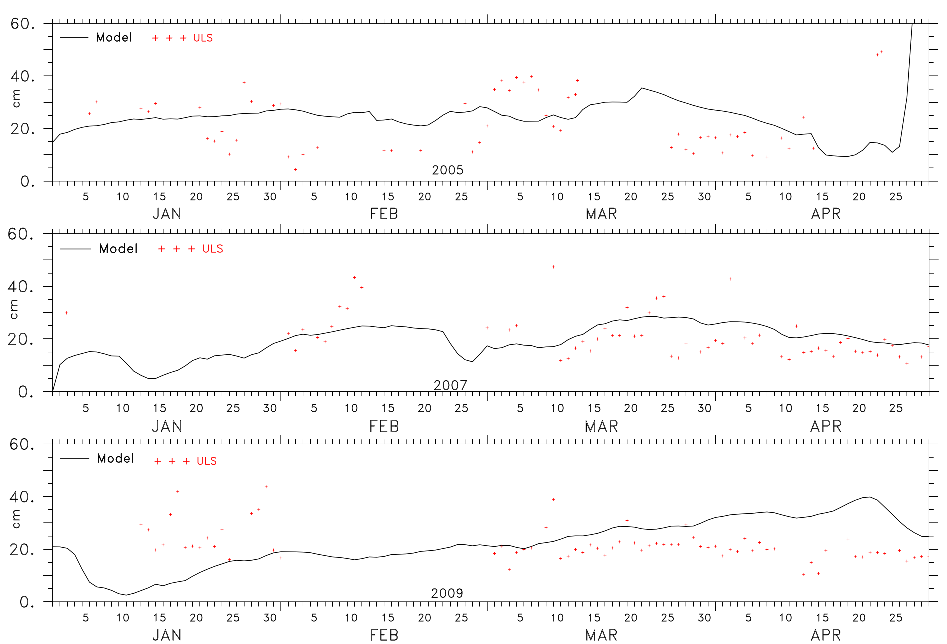

Figure 14. The level ice draft computed from the ULS measurement and the "M2" model estimated values at Makkovik Bank for 2005, 2007 and 2009.

The keel is computed using idealized sea ice floe comprising a system of two triangular sails and keels and a single melt pond (Tsamados et al., 2014). The ridge height is given by equation (4) and the correlation between the ridge height and keel depth is given by equation (5)

$$H_r = 2\frac{V_{rdg}}{A_{rdg}}\frac{(\alpha D_k m_k + \beta C m_r)}{(\phi_r m_k D_k + \phi_k m_r C^2)} \tag{4}$$

Where H_r is the ridge height, $m_r = tan(\alpha_r) = 0.4$, $\alpha_r = 21.8°$ is the slope of the sail and $m_k = tan(\alpha_k)$ = 0.5, $\alpha_k = 26.5°$ is the slope of the keel, ϕ_r is the porosity of the ridges, ϕ_k = $0.14 + 0.73\phi_r$ (Shokr and Sinha, 2015) is the porosity of the keels. $D_k = 5$ is the ratio distance between ridge to distance between the keels. V_{rdg} is the volume of the ridged ice, A_{rdg} is the ridged ice area fraction, α and β are the weight functions for area of ridged ice, C is the coefficient that relates ridge to keel and

$$H_k = CH_r \tag{5}$$

gives the keel depth H_k. The Makkovik Bank where the keel measurements are estimated from ULS has high variability of ice thickness, and frequency of the formation of keels are high due to the combined effect of the Labrador currents and winds, rafted ice are common in this region (Peterson I.K., 2013). Here the model and the observation of keel depth are used to estimate the parameter C.

The coefficient, C estimated for 2005, 2007 and 2009 shows that a value between 3.00 and 4.50 gives a good estimate of keel measurement for January and February while a value between 7.00 and 8.00 gives a good estimate for keel during March, April, and May. In Figure 15 the values of the coefficient C that relates ridge to keel for January and February is 3 and $C = 7.00$ for March, April and May, see equation (5). These values are derived under the assumptions in equation (4). The sensitivity of parameters has to be further explored to determine the characteristics of each parameter and its effect on the ridge, keel relationship which may result in a different conclusion. Since the interest lies in deriving this relationship from the assimilated model, so only results from M2 is presented. For non-assimilated model, the choice of parameters vary.

During January to February the formation of ice and ridges occurs, and during March the thick ice may be contributing towards the ridging thus increasing the value of C.

5.4 Freeboard

The uncertainty of freeboard measurements can arise due to the lack of leads. The presence of leads was ensured by selecting the regions where lead fraction derived from CryoSat-2 (Ricker et al., 2014) was greater than zero. In the model, freeboard is computed using equation (6) (Tsamados et al., 2014). For the region, the uncertainty of the freeboad measurements is below 40 cm (Ricker et al., 2014).

$$D_f = (v_{ice} + v_{sno})/A - D \tag{6}$$

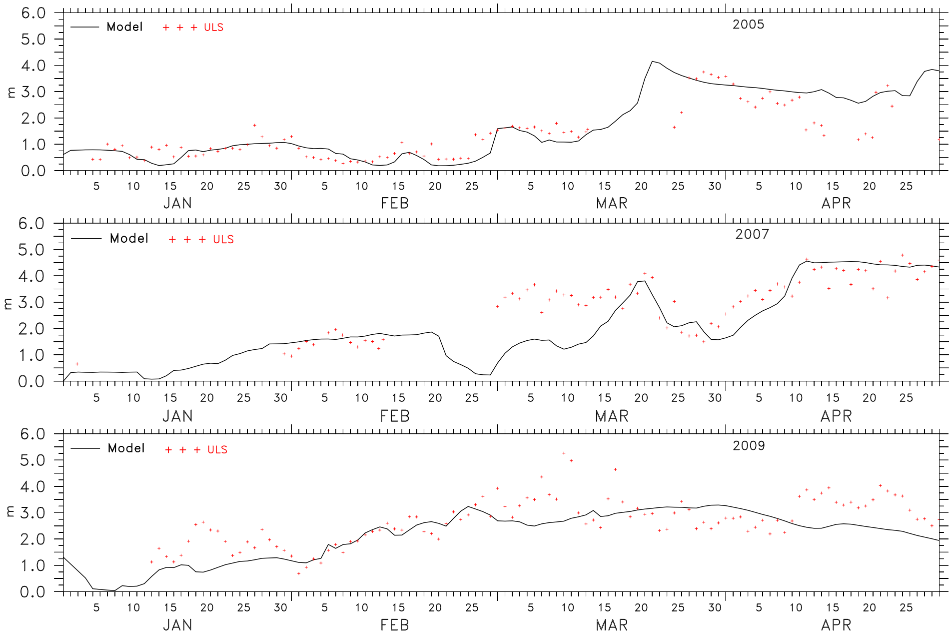

Figure 15. The keel depth computed from the ULS measurement and the "M2" model estimated values in cm for $2005, 2007$ and 2009.

Where v_{ice} is the volume of ice, v_{sno} is the volume of snow, A is the ice concentration, D is the draft, see equation (3).

The absolute mean difference between the model and the observation for January, February and March 2011 is shown in the Figure 16. M2 freeboard measurements are close to the observed freeboard. Figure 17 shows the RMSE of freeboard from model M2 and CryoSat-2 in the areas where the lead fraction was greater than zero. The RMSE is below the maximum uncertainty of 40 cm for the region of interest and was found to range between 4.5 cm and 11 cm. Figure 18 demonstrates the spatial estimates with M2, observation and uncertainty.

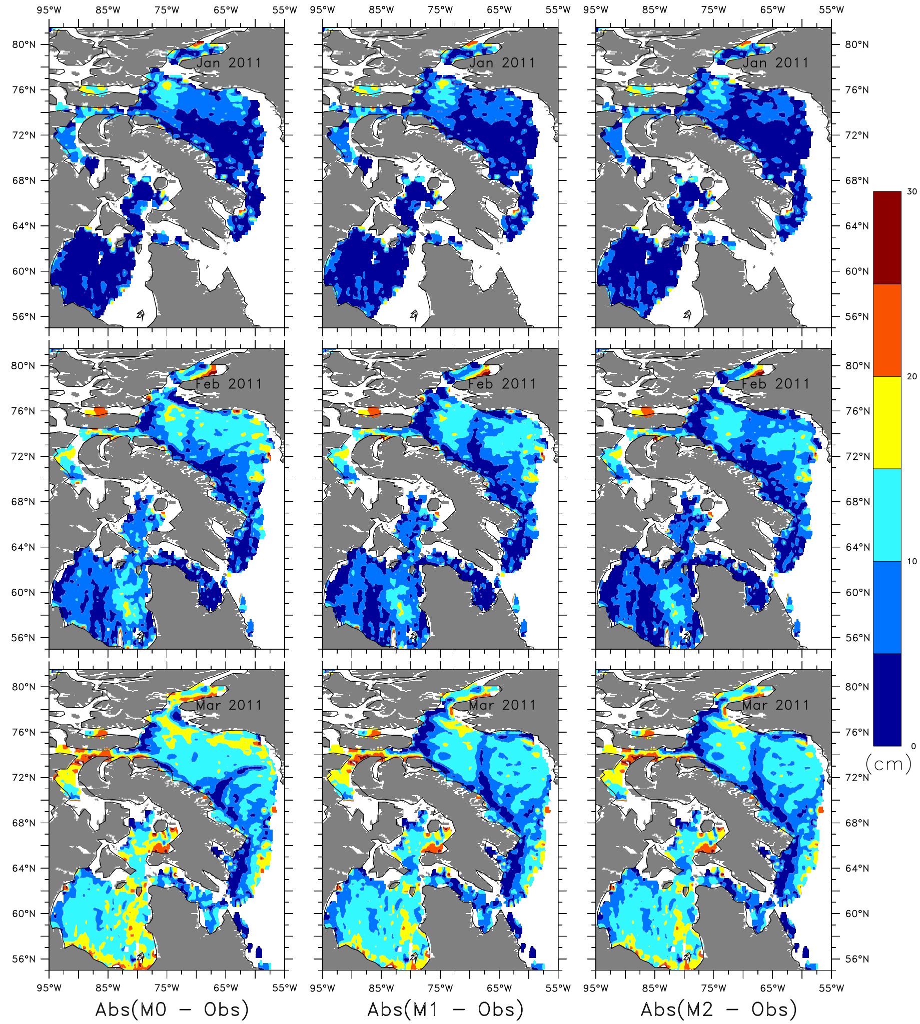

Figure 16. The absolute mean difference between the model freeboard for M0, M1 and M2 and CryoSat-2 for January, February and March 2011.

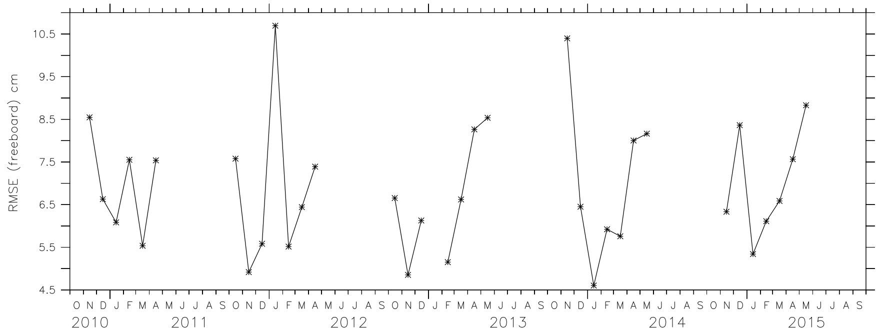

Figure 17. The RMSE of freeboard measure for the regions where the lead fraction is above 0%.

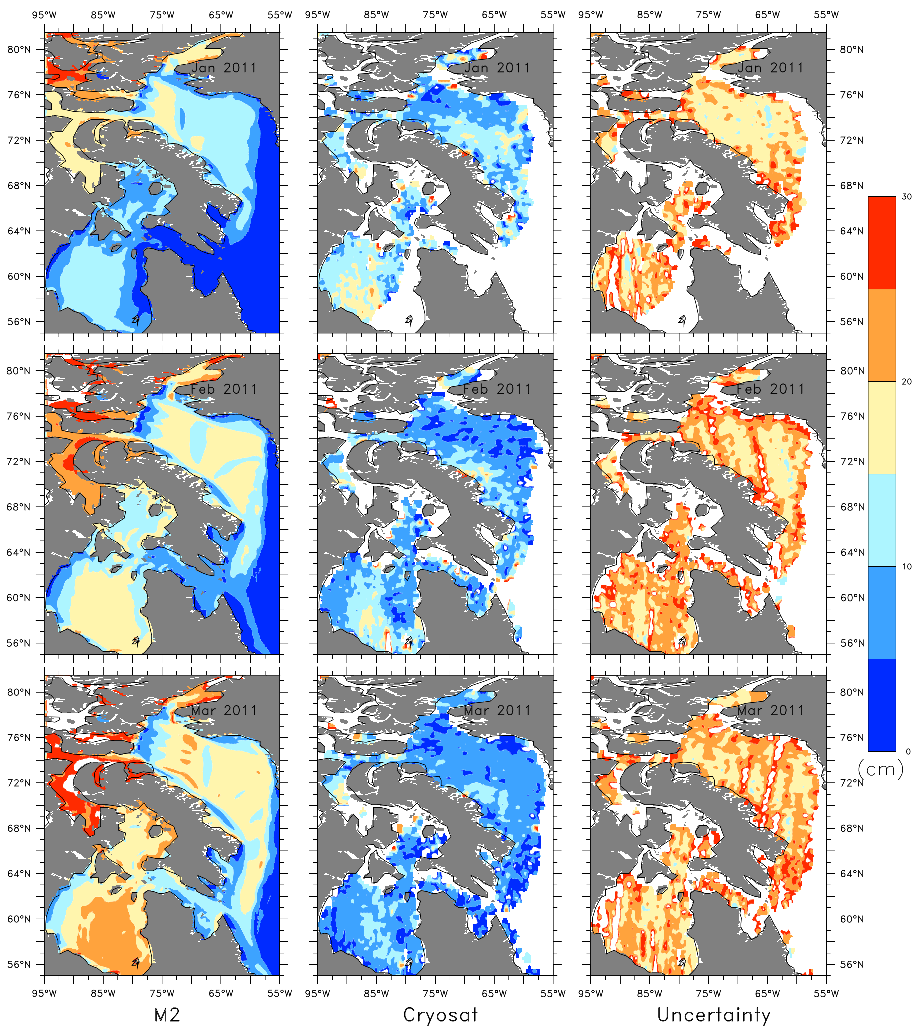

Figure 18. The Freeboard from model M2, CryoSat-2 and the uncertainty of the observations for January, February and Match 2011.

Figure 19 shows the observed freeboard from CryoSat-2, the uncertainty of observation, and the model M2. Only the model results from M2 are given since there are only slight deviations for M0 and M1 from the observation. Moreover, we are interested in the results of the assimilated model and how well it performs in the estimation of freeboard. The model values are within the uncertainty limits of the observation. Also, note that the model results are monthly averaged, while CryoSat-2 is a mosaic of daily measurements within a month. The spatial average of freeboard for the region, the observed value, and the uncertainty is shown in Figure 18. The average freeboard from the model lies within the uncertainty limits of the observation.

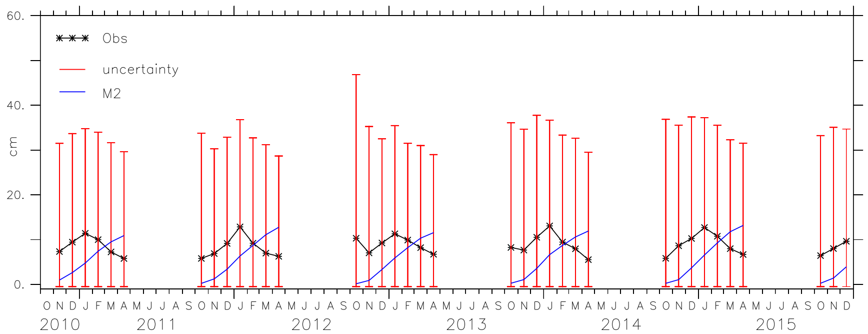

Figure 19. The freeboard from CryoSat-2, uncertainty of the observation and the model M2,

6 Conclusions

The assimilated models in the literature, and those implemented in forecasting centres use a constant drag formulation and lack the details on deriving the parameters other than ice concentration, and ice thickness (Lemieux et al., 2016; Rae et al., 2015). In this work a variable drag formulation is used for the friction associated with an effective sea ice surface roughness at the ice-atmosphere and ice-ocean interfaces and to compute the ice to ocean heat transfer. The results from the updated model were compared with satellite derived measurements to validate the model estimates of ice concentration, ice thickness, freeboard. Moreover, the model results were used to estimate relationship between sail and keel depth.

The modeled ice thickness demonstrated a good correspondence with the estimates from SMOS-MIRAS, except during the period of maximum ice extent. The deviation in the results of ice thickness during March have to be further explored by tuning the parameters that contribute to the ice thickness in the non assimilated model as well as the assimilation parameters. The thin ice category thicknesses are overestimated from October to November end but the values are within the uncertainty limits of SMOS from December to March. Also, the SMOS estimates are influenced by the presence of snow and also during the melt seasons the uncertainties of SMOS estimated ice thickness might increase in which case comparison with more reliable data would be required. The model freeboard are compared with estimates from CryoSat-2, and the RMSE was found to range between 4.5 cm and 11 cm. The estimates of freeboard from the model are within the uncertainty values of the CryoSat-2 (below 40 cm).

The level ice draft and keel values derived from ULS were compared with the modeled values. The coefficient that related the sail height and keel depth for the Makkovick region lies in a range $3-8$ depending on the period of the year. Since the variable drag formulation depends on the assimilation methodology further sensitivity studies has to be conduted for the optimisation of the model. The model will be made operational after further sensitivity studies.

Competing interests.

Acknowledgements. Funding support was provided by Research and Development Corporation (RDC), Newfoundland and Labrador. The authors also thank Tony King (C-CORE) and Ingrid Peterson (DFO, Government of Canada) for providing ULS data from Makkovik Bank. We also thank Center for Health Informatics and Analytics (CHIA), MUN and ACENet, Canada for providing computational resources. We would like to than the developers of CICE, the Los Alamos sea ice model for public availability of the sea ice model and the users group.

References

Barré, H. M., Duesmann, B., and Kerr, Y. H.: SMOS: The mission and the system, IEEE transactions on geoscience and remote sensing, 46, 587–593, 2008.

Bell, W.: A preprocessor for SSMIS radiances scientific description, Met Office, UK, 2006.

Bouzinac, C.: CryoSat product handbook, ESA User Manual, ESA, ESRIN, Italy, 4121, 4123, 2014.

Carsey, F. D.: Microwave remote sensing of sea ice, American Geophysical Union, 1992.

Caya, A., Buehner, M., Shokr, M., and Carrieres, T.: A first attempt of data assimilation for operational sea ice monitoring in Canada, in: Geoscience and Remote Sensing Symposium, 2006. IGARSS 2006. IEEE International Conference on, pp. 1705–1708, IEEE, 2006.

Caya, A., Buehner, M., and Carrieres, T.: Analysis and forecasting of sea ice conditions with three-dimensional variational data assimilation and a coupled ice–ocean model, Journal of Atmospheric and Oceanic Technology, 27, 353–369, 2010.

Deutch, R.: Estimation theory, Prentice-Hall, Upper Sadddle River, NJ, 1965.

Dzierzbicka-Głowacka, L., Janecki, M., Nowicki, A., and Jakacki, J.: Activation of the operational ecohydrodynamic model (3D CEMBS)–the ecosystem module, Oceanologia, 55, 543–572, 2013.

Fenty, I. and Heimbach, P.: Coupled sea ice–ocean-state estimation in the Labrador Sea and Baffin Bay, Journal of Physical Oceanography, 43, 884–904, 2013.

Hunke, E. C., Lipscomb, W. H., Turner, A. K., Jeffery, N., and Elliott, S.: CICE: the Los Alamos Sea Ice Model Documentation and Software User's Manual Version 5.1 LA-CC-06-012, T-3 Fluid Dynamics Group, Los Alamos National Laboratory, 675, 2015.

Kaleschke, L., Tian-Kunze, X., Maaß, N., Mäkynen, M., and Drusch, M.: Sea ice thickness retrieval from SMOS brightness temperatures during the Arctic freeze-up period, Geophysical Research Letters, 39, 2012.

Kaleschke, L., Tian-Kunze, X., Maaß, N., Heygster, G., Huntemann, M., Wang, H., and Haas, C.: SMOS Sea Ice Retrieval Study (SMOSIce), ESA Support To Science Element (STSE), Final Report ESA ESTEC contract no, Tech. rep., 4000101476/10/NL/CT, 2013.

Karvonen, J., Cheng, B., Vihma, T., Arkett, M., and Carrieres, T.: A method for sea ice thickness and concentration analysis based on SAR data and a thermodynamic model, The Cryosphere, 6, 1507–1526, 2012.

Kerr, Y. H., Waldteufel, P., Wigneron, J.-P., Martinuzzi, J., Font, J., and Berger, M.: Soil moisture retrieval from space: The Soil Moisture and Ocean Salinity (SMOS) mission, IEEE transactions on Geoscience and remote sensing, 39, 1729–1735, 2001.

Kubat, I., Sayed, M., Savage, S. B., and Carrieres, T.: Numerical simulations of ice thickness redistribution in the Gulf of St. Lawrence, Cold Regions Science and Technology, 60, 15–28, 2010.

Lemieux, J.-F., Beaudoin, C., Dupont, F., Roy, F., Smith, G. C., Shlyaeva, A., Buehner, M., Caya, A., Chen, J., Carrieres, T., et al.: The Regional Ice Prediction System (RIPS): verification of forecast sea ice concentration, Quarterly Journal of the Royal Meteorological Society, 142, 632–643, 2016.

Levitus, S. et al.: The world ocean database, Data Science Journal, 12, WDS229–WDS234, 2013.

Lindsay, R. and Zhang, J.: Assimilation of ice concentration in an ice–ocean model, Journal of Atmospheric and Oceanic Technology, 23, 742–749, 2006.

Mesinger, F., DiMego, G., Kalnay, E., Mitchell, K., Shafran, P. C., Ebisuzaki, W., Jović, D., Woollen, J., Rogers, E., Berbery, E. H., et al.: North American regional reanalysis, Bulletin of the American Meteorological Society, 87, 343–360, 2006.

Peterson I.K., Prinsenberg S.J., B. D.: Sea-ice draft and velocities from moorings on the Labrador Shelf(Makkovik Bank): 2003-2011, 2013.

Petty, A. A., Holland, P. R., and Feltham, D. L.: Sea ice and the ocean mixed layer over the Antarctic shelf seas, Cryosphere, 8, 761–783, 2014.

Prasad, S., Zakharov, I., Bobby, P., and McGuire, P.: The implementation of sea ice model on a regional high-resolution scale, Ocean Dynamics, 65, 1353–1366, 2015.

Prasad, S., Zakharov, I., Bobby, P., Power, D., McGuire, P., et al.: Model Based Estimation of Sea Ice Parameters, in: Arctic Technology Conference, Offshore Technology Conference, 2016.

Rae, J., Hewitt, H., Keen, A., Ridley, J., West, A., Harris, C., Hunke, E., and Walters, D.: Development of the Global Sea Ice 6.0 CICE configuration for the Met Office Global coupled model, Geoscientific Model Development, 8, 2221–2230, 2015.

Reynolds, R. W., Smith, T. M., Liu, C., Chelton, D. B., Casey, K. S., and Schlax, M. G.: Daily high-resolution-blended analyses for sea surface temperature, Journal of Climate, 20, 5473–5496, 2007.

Ricker, R., Hendricks, S., Helm, V., Skourup, H., and Davidson, M.: Sensitivity of CryoSat-2 Arctic sea-ice freeboard and thickness on radar-waveform interpretation, Cryosphere, 8, 1607–1622, 2014.

Ricker, R., Hendricks, S., Kaleschke, L., and Tian-Kunze, X.: CS2SMOS: Weekly Arctic Sea-Ice Thickness Data Record, 2016.

Ross, E., Fissel, D., Wyatt, G., Milutinovic, N., and Lawrence, J.: Project report: Data processing and analysis of the ice draft and ice velocity, Makkovik Bank, 2014.

Sayed, M., Carrieres, T., et al.: Overview of a new operational ice model, in: The Ninth International Offshore and Polar Engineering Conference, International Society of Offshore and Polar Engineers, 1999.

Sayed, M., Savage, S., and Carrieres, T.: Examination of Ice Ridging Methods Using Discrete Particles, in: Proceedings 16th International Conference on Port and Ocean Engineering under Arctic Conditions (POAC'01), pp. 1087–1096, 2001.

Sayed, M., Carrieres, T., Tran, H., Savage, S. B., et al.: Development of an operational ice dynamics model for the Canadian Ice Service, in: The Twelfth International Offshore and Polar Engineering Conference, International Society of Offshore and Polar Engineers, 2002.

Scagliola, M.: CryoSat footprints Aresys technical note, SAR-CRY2-TEN-6331, Aresys/ESA, Italy, 2013.

Shokr, M. and Sinha, N.: Sea ice: physics and remote sensing, John Wiley & Sons, 2015.

Smith, T. M.: A long-term record of blended satellite and in situ sea-surface temperature for climate monitoring, modeling and environmental studies, Earth System Science Data, 8, 165, 2016.

Spreen, G., Kaleschke, L., and Heygster, G.: Sea ice remote sensing using AMSR-E 89-GHz channels, Journal of Geophysical Research: Oceans, 113, 2008.

Stirling, I.: The biological importance of polynyas in the Canadian Arctic, Arctic, pp. 303–315, 1980.

Tian-Kunze, X. and Kaleschke, L.: Read-me-first note for the release of the SMOS Level 3 ice thickness data product, University of Hamburg, 2016.

Tian-Kunze, X., Kaleschke, L., Maaß, N., Mäkynen, M., Serra, N., Drusch, M., and Krumpen, T.: SMOS-derived thin sea ice thickness: algorithm baseline, product specifications and initial verification, Cryosphere, 8, 997–1018, 2014.

Tietsche, S., Balmaseda, M., Zuo, H., and de Rosnay, P.: Comparing Arctic Winter Sea-ice Thickness from SMOS and ORAS5, European Centre for Medium-Range Weather Forecasts, 2017.

Tietsche, S., Alonso-Balmaseda, M., Rosnay, P., Zuo, H., Tian-Kunze, X., and Kaleschke, L.: Thin sea ice in the Arctic: comparing L-band radiometry retrievals with an ocean reanalysis, Cryosphere, 12, 2051–2018, 2018.

Tonboe, R., Lavelle, J., Pfeiffer, R.-H., and Howe, E.: Product User Manual for OSI SAF Global Sea Ice Concentration, 2016.

Tsamados, M., Feltham, D. L., Schroeder, D., Flocco, D., Farrell, S. L., Kurtz, N., Laxon, S. W., and Bacon, S.: Impact of variable atmospheric and oceanic form drag on simulations of Arctic sea ice, Journal of Physical Oceanography, 44, 1329–1353, 2014.

Wang, K., Debernard, J., Sperrevik, A. K., Isachsen, P. E., and Lavergne, T.: A combined optimal interpolation and nudging scheme to assimilate OSISAF sea-ice concentration into ROMS, Annals of Glaciology, 54, 8–12, 2013.

Zhou, L., Xu, S., Liu, J., and Wang, B.: On the retrieval of sea ice thickness and snow depth using concurrent laser altimetry and L-band remote sensing data, The Cryosphere, 12, 993–1012, 2018.